Open Access | Baghdad Science Journal | P-ISSN: 2078-8665
Published Online First: January 2021 | E-ISSN: 2411-7986

DOI: http://dx.doi.org/10.21123/bsj.2021.18.2.0279

Influence of Varying Temperature and Concentration on Magnetohydrodynamics Peristaltic Transport for Jeffrey Fluid with a Nanoparticles Phenomenon through a Rectangular Porous Duct

Dheia G. Salih Al-Khafajy

Department of Mathematics, College of Science, University of Al-Qadisiyah, Diwaniya, Iraq.
E-mail: dheia.salih@qu.edu.iq
ORCID ID: https://orcid.org/0000-0001-7848-8243

Received 18/9/2019, Accepted 27/4/2020, Published Online First 11/1/2021, Published 1/6/2021

This work is licensed under a Creative Commons Attribution 4.0 International License.

Abstract:

A mathematical model constructed to study the combined effects of the concentration and the thermodiffusion on the nanoparticles of a Jeffrey fluid with a magnetic field effect the process of containing waves in a three-dimensional rectangular porous medium canal. Using the HPM to solve the nonlinear and coupled partial differential equations. Numerical results were obtained for temperature distribution, nanoparticles concentration, velocity, pressure rise, pressure gradient, friction force and stream function. Through the graphs, it was found that the velocity of fluid rises with the increase of a mean rate of volume flow and a magnetic parameter, while the velocity goes down with the increasing a Darcy number and lateral walls. Also, the velocity behaves strangely under the influence of the Brownian motion parameter and local nanoparticle Grashof number effect.

Key words: Homotopy perturbation method (HPM), Jeffrey fluid, Magnetohydrodynamics (MHD), Nanoparticles, Peristaltic flow.

Introduction:

The Peristaltic flow is a mechanics for pumped fluids into tubes when the wave-out of the contraction zone or expansion spreads along an expandable and shrinking tube containing fluid. The peristalses have very important applications in many industries and physiological systems. They include the transfer of urine and food through the urinary tract and digestive system respectively, blood circulation through blood movement, the menstrual movement for the egg in the fallopian tube. The major industrial application for this phenomenon is the design of rotary pumps used in pumping fluids without contamination due to contact with pumping munitions (1). Furthermore, the peristaltic movement study has acquired many applications, for example, ship movements, mud transport, sensitive or corrosive liquids, healthy fluids, and harmful fluids in the nuclear industry. In (2) Kothandapani and Srinivas analyzed the effect of a magnetic field in the peristaltic transport for a Jeffrey fluid in an asymmetric canal and discussed the problem in wave frame moved at a stable axial velocity under the approximations of low Reynolds number and long wavelength. The influence of wall properties and heat transfer on the peristaltic transport of a Jeffrey fluid through a porous medium in the magnetic field has been investigated by Al-Khafajy and Abdulhadi in (3). The effect of lateral walls on peristaltic flow in a rectangular duct has been investigated by (4). They noted that the uterine cross-section of the uterus may be preferably approximated by a tube than a rectangular section of a two-dimensional canal. Nadeem et al. (5) analyzed a "mathematical model for the peristaltic flow of Jeffrey fluid with nanoparticles phenomenon through a rectangular duct".

Nanotechnology has basic and important applications in the modern industry in nano-size exhibit unmatched physical and chemical properties. Gasoline, oil, ethylene glycol and water are common examples of essential fluids used for liquid nanoparticles. Nano-fluids make a huge contribution to heat transfer such as fuel cells, microelectronics, hybrid engines, refrigerators, nuclear reactor radiators, space technology and many other cases. Suitable to the spacious thermal properties, nanofluid has attracted the consideration of researchers to the fabrication of heat transfer fluids in hotness exchangers, in plants and in auto cooling chillers. In literature, many researchers and industrialists are studied nanofluid and their applications, (6-11). Nadeem and Maraj (6) described the mathematical analysis for peristaltic flow of a nanofluid in a curved channel with compliant walls. Hayat et al. (7) investigated the flow of MHD from a saturated porous space of Williamson fluid. The effect of thermal radiation on unstable free heat flow (MHD) for the rotation of Jeffrey nanofluid that passes through the porous medium was studied in (8). In (9) Latha and Kumar described the mathematical analysis to study the effects of Joule heating and Hall current by heat radiation on the peristaltic flow of a nanofluid in a channel with flexible walls. In (10) Hayat et al. investigated the magneto peristalsis of Jeffrey nanomaterial in vertical asymmetric compliant channel walls with considering nonlinear thermal radiation. In (11) Ansari et al. analyzed the problem of unstable laminar boundary layer flow, caused by propellant expansion sheet and thermal transfer to Jeffrey nanofluid.

Stimulated by this, assume a mathematical model for analyzing the combined effects of concentration and heat diffusion on nanoparticles with the influence of the magnetic field on the process of containing waves in a rectangular porous medium channel in 3D. This paper consists of five sections, the first section includes formulating the governing equations with the boundary conditions in addition to displaying the dimensionless transformations for facilitation the governing equations with assuming a very small Reynolds number or a very large wavelength to solve the problem. In the second section, the dimensionless equations are analytically solved by the HPM, the expressions are obtained for velocity profile, temperature distribution, pressure rise, pressure gradient, nanoparticles concentration and friction force. The third section includes the effects of various emerging parameters that are discussed through graphs in detail. The fourth section discusses the trapping phenomenon and the parameters that affect the increase and decrease, appear or disappear of the trapping bolus. The last section briefly reviews the most important parameters (Schmidt number, Grashof number, Prandtl number, Darcy number, magnetic parameter) that affect the movement of the fluid.

Mathematical formulation:

Considered the peristaltic flow of a non-Newtonian (Jeffrey) incompressible fluid with the concentration of nanoparticles in a cross-section of a normal rectangular three-dimensional canal (4). The flow is generated by the propagation of sinusoidal waves along the axial direction of the canal with c (constant velocity), Fig.1.

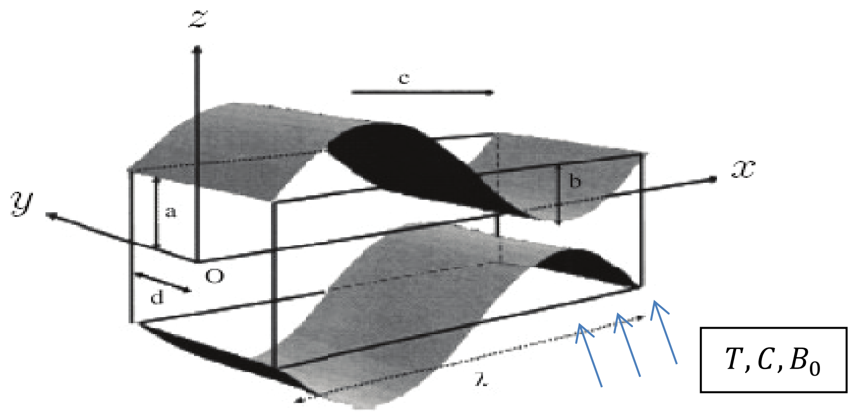

Figure 1. Schematic diagram for peristaltic flow in a rectangular duct

The peristaltic waves on the walls as represented (4):

$$Z = \mp H(X,t) = \mp a \mp b\cos\left[\frac{2\pi}{\lambda}(X - ct)\right] \quad \dots\ (1)$$

whereas a and b are wave amplitudes, t is time and X is the wave propagation direction.

The walls are still parallel to XZ-plane that is unobstructed and not subject to any wave movement. Assuming that the side speed is zero as there is no change in the lateral direction of the transverse channel, that is $V = (U, 0, W)$. The governing equations in three-dimensional for flow velocity of the nanofluid problem has the following form:

$$\frac{\partial U}{\partial X} + \frac{\partial W}{\partial \bar{Z}} = 0 \quad \dots\ (2)$$

$$\rho_f\left(\frac{\partial U}{\partial t} + U\frac{\partial U}{\partial X} + W\frac{\partial U}{\partial Z}\right) = -\frac{\partial P}{\partial X} + \frac{\partial S_{XX}}{\partial X} + \frac{\partial S_{XY}}{\partial Y} + \frac{\partial S_{XZ}}{\partial Z} + \rho_f g \alpha_f(\bar{T} - T_0) + \rho_f g \alpha_f(\bar{C} - C_0) - \frac{\mu}{k}U - \sigma B_0^2 U \quad \dots\ (3)$$

$$0 = -\frac{\partial P}{\partial Y} + \frac{\partial S_{YX}}{\partial X} + \frac{\partial S_{YY}}{\partial Y} + \frac{\partial S_{YZ}}{\partial Z} \quad \dots\ (4)$$

$\rho_f\left(\frac{\partial W}{\partial t}+U\frac{\partial W}{\partial X}+W\frac{\partial W}{\partial Z}\right)=-\frac{\partial P}{\partial Z}+\frac{\partial S_{ZX}}{\partial X}+\frac{\partial S_{ZY}}{\partial Y}+\frac{\partial S_{ZZ}}{\partial Z}-\frac{\mu}{k}W-\sigma B_0^2 W$ … (5)

$\frac{\partial \bar{T}}{\partial \bar{t}}+U\frac{\partial \bar{T}}{\partial X}+W\frac{\partial \bar{T}}{\partial Z}=\propto\left(\frac{\partial^2 \bar{T}}{\partial X^2}+\frac{\partial^2 \bar{T}}{\partial Y^2}+\frac{\partial^2 \bar{T}}{\partial Z^2}\right)+\tau\left\{D_B\left(\frac{\partial \bar{C}}{\partial X}\frac{\partial \bar{T}}{\partial X}+\frac{\partial \bar{C}}{\partial Y}\frac{\partial \bar{T}}{\partial Y}+\frac{\partial \bar{C}}{\partial Z}\frac{\partial \bar{T}}{\partial Z}\right)+\frac{D_T}{T_m}\left(\left(\frac{\partial \bar{T}}{\partial X}\right)^2+\left(\frac{\partial \bar{T}}{\partial Y}\right)^2+\left(\frac{\partial \bar{T}}{\partial Z}\right)^2\right)\right\}$… (6) $\frac{\partial \bar{C}}{\partial \bar{t}}+U\frac{\partial \bar{C}}{\partial X}+W\frac{\partial \bar{C}}{\partial Z}=D_B\left(\frac{\partial^2 \bar{C}}{\partial X^2}+\frac{\partial^2 \bar{C}}{\partial Y^2}+\frac{\partial^2 \bar{C}}{\partial Z^2}\right)+\frac{D_T}{T_0}\left(\frac{\partial^2 \bar{T}}{\partial X^2}+\frac{\partial^2 \bar{T}}{\partial Y^2}+\frac{\partial^2 \bar{T}}{\partial Z^2}\right)$
… (7)

where U is the component of the velocity in X-direction, W is the component of the velocity in Z-direction, T is the temperature, C is the concentration of the fluid, μ is the dynamic viscosity, k is the permeability, B_0 is the magnetic field, σ is the electrical conductivity, K is the thermal conductivity, c_p is the specific heat capacity at constant pressure, D_T is the coefficient of mass diffusivity, T_m is the mean fluid temperature and $\tau=\frac{(\rho c)p}{(\rho c)_f}$ is the ratio of the active thermal capacity of the nanoparticle to the thermal capacity of the base fluid. Also S represents the structural relations for Jeffrey fluid (12):

$S=\frac{\mu}{1+\lambda_1}(\dot{\gamma}+\lambda_2\ddot{\gamma}),$ … (8)

where $\lambda_1$the ratio of relaxation to retardation times, $\dot{\gamma}$ is the shear rate, λ_2 is the retardation time and μ is the viscosity of the fluid.

To analyze the flow of the (x,y,z) current wave frame with the constant velocity c away from the (X,Y,Z) fixed frame by the transference

$x=X-ct,\ y=Y,\ z=Z,\ u=U-c,\ w=W,\ p(x,z)=P(X,Z,T),\ T=\bar{T},\ C=\bar{C}$… (9)

Introducing the following dimensionless transformations for facilitating the governing equations of the motion, as follows:

$$\left.\begin{array}{l}\bar{x}=\frac{x}{\lambda},\bar{y}=\frac{y}{d},\bar{z}=\frac{z}{a},\bar{t}=\frac{ct}{\lambda},\bar{u}=\frac{u}{c},\bar{w}=\frac{w}{c\delta},\delta=\frac{a}{\lambda},\bar{p}=\frac{a^2p}{\mu\lambda c},\bar{S}=\frac{aS}{\mu c},\propto=\frac{K}{(\rho c)_f},Da=\frac{K}{a^2}\\ S_c=\frac{\mu}{\rho D_B},R_e=\frac{\rho ca}{\mu},\emptyset=\frac{b}{a},\theta=\frac{T-T_0}{T_1-T_0},\Omega=\frac{C-C_0}{C_1-C_0},\bar{h}=\frac{H}{c},\beta=\frac{a}{d},B_r=\frac{\rho_f g\alpha_f a^2(C_1-C_0)}{\mu c},\\ P_r=\frac{\mu}{\rho\propto},N_b=\frac{\tau D_B(C_1-C_0)}{\propto},N_t=\frac{D_T(T_1-T_0)}{T_0\propto},G_r=\frac{\rho_f g\alpha_f a^2(T_1-T_0)}{\mu c},M^2=\frac{\sigma a^2B_0^2}{\mu}\end{array}\right\}\quad \dots (10)$$

where R_e, S_c, N_b, N_t, B_r, G_r, P_r, Da and M represent the Reynolds number, the Schmidt number, the Brownian motion parameter, the thermophoresis parameter, local nanoparticle Grashof number, local temperature Grashof number, Prandtl number, Darcy number and the magnetic parameter.

Compensate equations (10) into equations (1)-(9), and using the assumption of long-wavelength $\delta\ll 1$ and low Reynolds number, lead to simplifying the equations to the following form:

$\frac{\partial u}{\partial x}+\frac{\partial w}{\partial z}=0$ … (11)

$\beta^2\frac{\partial^2 u}{\partial y^2}+\frac{\partial^2 u}{\partial z^2}-(1+\lambda_1)\left(\frac{1}{Da}+M^2\right)u=(1+\lambda_1)\left(\frac{1}{Da}+M^2+\frac{\partial p}{\partial x}-G_r\theta-B_r\Omega\right)$ … (12)

$\frac{\partial p}{\partial y}=0\ ,\ \frac{\partial p}{\partial z}=0$ … (13)

$\beta^2\frac{\partial^2 \theta}{\partial y^2}+\frac{\partial^2 \theta}{\partial z^2}+N_b\left(\beta^2\frac{\partial \Omega}{\partial y}\frac{\partial \theta}{\partial y}+\frac{\partial \Omega}{\partial z}\frac{\partial \theta}{\partial z}\right)+N_t\left(\beta^2\left(\frac{\partial \theta}{\partial y}\right)^2+\left(\frac{\partial \theta}{\partial z}\right)^2\right)=0$ … (14)

$\beta^2\frac{\partial^2 \Omega}{\partial y^2}+\frac{\partial^2 \Omega}{\partial z^2}+\frac{N_t}{N_b}\left(\beta^2\frac{\partial^2 \theta}{\partial y^2}+\frac{\partial^2 \theta}{\partial z^2}\right)=0$ … (15)

The boundaries of the channel will obtain the dimensionless form as follows:

$z=\mp h(x)=\mp 1\mp\emptyset\, cos2\pi x$ … (16)

The corresponding boundary conditions are:

$u=-1$ at $y=\mp 1$, $u=-1$ at $z=\mp h(x)$,
… (17)

$\theta=a_1,\ \Omega=a_2$ at $y=1$, $\theta=b_1,\ \Omega=b_2$ at $y=-1$, … (18)

$\theta=\ \Omega=0$ at $z=h(x)$, $\theta=\Omega=1$ at $z=-h(x)$ … (19)

The statements for the dimensionless flow functions can be described as $u=\frac{\partial\psi}{\partial z},\ w=\frac{\partial\psi}{\partial x}$ where ψ represents the flow function.

Problem solving by HPM:

The solution of the nonlinear partial differential equations (11)-(15) have been found by the HPM. The deformity equations for the problem are defined as (Ji-Huan, 2010).

$\mathcal{H}(v,r)=\mathcal{V}[v]-\mathcal{V}[\tilde{u}_0]+r\mathcal{V}[\tilde{u}_0]+r\left\{\beta^2\frac{\partial^2 v}{\partial y^2}-(1+\lambda_1)\left(\left(\frac{1}{Da}+M^2\right)(v+1)+\frac{\partial p}{\partial x}-G_r\Theta-B_r\Omega\right)\right\}=0,$… (20)

$\mathcal{H}(\Theta,r)=\mathcal{V}[\Theta]-\mathcal{V}[\tilde{\theta}_0]+r\mathcal{V}[\tilde{\theta}_0]+r\left\{\beta^2\frac{\partial^2 \Theta}{\partial y^2}+N_b\left(\beta^2\frac{\partial \Phi}{\partial y}\frac{\partial \Theta}{\partial y}+\frac{\partial \Phi}{\partial z}\frac{\partial \Theta}{\partial z}\right)+N_t\left(\beta^2\left(\frac{\partial \Theta}{\partial y}\right)^2+\left(\frac{\partial \Theta}{\partial z}\right)^2\right)\right\}=0,$ … (21)

$\mathcal{H}(\Phi,r)=\mathcal{V}[\Phi]-\mathcal{V}[\tilde{\Omega}_0]+r\mathcal{V}[\tilde{\Omega}_0]+r\left\{\beta^2\frac{\partial^2 \Phi}{\partial y^2}+\frac{N_t}{N_b}\left(\beta^2\frac{\partial^2 \Theta}{\partial y^2}+\frac{\partial^2 \Theta}{\partial z^2}\right)\right\}=0.$ … (22)

Here, r is the parameter included that has the range $0\le r\le 1$, provided that for $r=0$, obtained the primary solution and for $r=1$, reached the final solution. Here, $\mathcal{V}$ is the linear operator that is taken here as $\mathcal{V}=\frac{\partial^2}{\partial z^2}$. Choosing the following preliminary estimates

$$\tilde{u}_0(y,z)=\frac{1}{\beta^2}(1-y^2)(z^2-h^2)-1, \quad \dots (23)$$

$$\tilde{\theta}_0=\tilde{\Omega}_0=\beta^2(z^2-h^2)+\frac{h-z}{2h}. \quad \dots (24)$$

Let us define

$$\left.\begin{aligned} v(x,y,z)&=v_0+rv_1+r^2v_2+\cdots\\ \Theta(x,y,z)&=\Theta_0+r\Theta_1+r^2\Theta_2+\cdots\\ \Phi(x,y,z)&=\Phi_0+r\Phi_1+r^2\Phi_2+\cdots\end{aligned}\right\} \quad \dots (25)$$

Replacing the equations (25) into equations (20)–(22) and then the similar forces are compared with r, the following problems are produced with corresponding boundary conditions, i.e.

For r^0:

$\mathcal{V}[v_0]-\mathcal{V}[\tilde{u}_0]=0$, with $v_0=-1$ at $y=\mp 1$, $v_0=-1$ at $z=\mp h(x)$,

$\mathcal{V}[\Theta_0]-\mathcal{V}[\tilde{\theta}_0]=0$, with $\Theta_0=a_1$ at $y=1$, $\Theta_0=b_1$ at $y=-1$, $\Theta_0=0$ at $z=h(x)$, $\Theta_0=1$ at $z=-h(x)$,

$\mathcal{V}[\Phi_0]-\mathcal{V}[\tilde{\Omega}_0]=0$, with $\Phi_0=a_2$ at $y=1$, $\Phi_0=b_2$ at $y=-1$, $\Phi_0=0$ at $z=h(x)$, $\Phi_0=1$ at $z=-h(x)$.

For r^1: $\frac{\partial^2 v_1}{\partial z^2}+\beta^2\frac{\partial^2 v_0}{\partial y^2}+\frac{\partial^2 v_0}{\partial z^2}-(1+\lambda_1)\left(\left(\frac{1}{Da}+M^2\right)(v_0+1)+\frac{\partial p}{\partial x}-G_r\Theta_0-B_r\Phi_0\right)=0,$

$$\frac{\partial^2\Theta_1}{\partial z^2}+\beta^2\frac{\partial^2\Theta_0}{\partial y^2}+\frac{\partial^2\Theta_0}{\partial z^2}+N_b\left(\beta^2\frac{\partial\Theta_0}{\partial y}\frac{\partial\Phi_0}{\partial y}+\frac{\partial\Theta_0}{\partial z}\frac{\partial\Phi_0}{\partial z}\right)+N_t\left(\beta^2\left(\frac{\partial\Theta_0}{\partial y}\right)^2+\left(\frac{\partial\Theta_0}{\partial z}\right)^2\right)=0,$$

$$\frac{\partial^2\Phi_1}{\partial z^2}+\beta^2\frac{\partial^2\Phi_0}{\partial y^2}+\frac{\partial^2\Phi_0}{\partial z^2}+\frac{N_t}{N_b}\left(\beta^2\frac{\partial^2\Theta_0}{\partial y^2}+\frac{\partial^2\Theta_0}{\partial z^2}\right)=0.$$

with $v_1=\Theta_1=\Phi_1=0$ at $y=\mp 1$, $v_1=\Theta_1=\Phi_1=0$ at $z=\mp h(x)$,

For r^2: $\frac{\partial^2 v_2}{\partial z^2}+\beta^2\frac{\partial^2 v_1}{\partial y^2}-(1+\lambda_1)\left(\left(\frac{1}{Da}+M^2\right)v_1-G_r\theta_1-B_r\vartheta_1\right)=0,$

$$\frac{\partial^2\Theta_2}{\partial z^2}+\beta^2\frac{\partial^2\Theta_1}{\partial y^2}+N_b\left(\beta^2\frac{\partial\Theta_1}{\partial y}\frac{\partial\Phi_0}{\partial y}+\frac{\partial\Theta_1}{\partial z}\frac{\partial\Phi_0}{\partial z}+\frac{\partial\Theta_0}{\partial y}\frac{\partial\Phi_1}{\partial y}+\frac{\partial\Theta_0}{\partial z}\frac{\partial\Phi_1}{\partial z}\right)=0,$$

$$\frac{\partial^2\Phi_2}{\partial z^2}+\beta^2\frac{\partial^2\Phi_1}{\partial y^2}+\frac{N_t}{N_b}\left(\beta^2\frac{\partial^2\Theta_1}{\partial y^2}+\frac{\partial^2\Theta_1}{\partial z^2}\right)=0.$$

with $v_2=\Theta_2=\Phi_2=0$ at $y=\mp 1$, $v_2=\Theta_2=\Phi_2=0$ at $z=\mp h(x)$,

The corresponding solutions for the above equation systems determines after three iterations and uses equations (25) as

$$u=\lim_{r\to 1}v=v_0+v_1+v_2+\cdots$$
$$\theta=\lim_{r\to 1}\Theta=\Theta_0+\Theta_1+\Theta_2+\cdots$$
$$\Omega=\lim_{r\to 1}\Phi=\Phi_0+\Phi_1+\Phi_2+\cdots$$

Obtained:

$$\begin{aligned}&u(x,y,z)=\frac{1}{\beta^2}(1-y^2)(z^2-h^2)-1+\frac{h^2(1+\lambda_1)}{12Da\beta^2}\left[h^2(1+DaM^2)(y^2-1)+Da\beta^2(B_r+G_r)(5\beta^2-3)+6Da\beta^2+\frac{\partial p}{\partial x}\right]+\\&\frac{h^2(1+\lambda_1)}{144Da\beta^2N_b}\Big\{h^2N_b(1+\lambda_1)(1+DaM^2)\Big[Da\beta^2(B_r+G_r)(244\beta^2-150)+244h^2(1+DaM^2)(y^2-1)+300Da\beta^2(B_r+G_r)\frac{\partial p}{\partial x}\Big]+Da\beta^2(1+\\&\lambda_1)[600h^2Da\beta^2(B_rN_t+B_rN_b+G_rN_b)-244h^4\beta^2N_b(1+DaM^2)+DaN_bG_r(N_t+N_b)(75+244h^4\beta^2)]\Big\}-\frac{1}{2}h(B_r+G_r)(1+\lambda_1)z+\\&\frac{z^2(1+\lambda_1)}{4Da\beta^2}\left[2h^2(1+DaM^2)(y^2-1)+Da\beta^2(B_r+G_r)(2h^2\beta^2-1)+2Da\beta^2\frac{\partial p}{\partial x}\right]+\frac{z^3(B_r+G_r)(1+\lambda_1)}{12h}-\\&\frac{z^2(1+\lambda_1)}{12Da\beta^2}[Da\beta^4(B_r+G_r)+(1+DaM^2)(y^2-1)+Da\beta^2]+\frac{7h^3(1+\lambda_1)z}{720Da}[4Da\beta^2G_r(N_t+N_b)-(1+\lambda_1)(1+DaM^2)(B_r+G_r)]+\\&\frac{(1+\lambda_1)z^2}{48Da^2\beta^2N_b}\Big[h^2N_b(1+\lambda_1)(1+DaM^2)+10h^2(1+DaM^2)(y^2-1)+10Dah^2\beta^4(B_r+G_r)-6Da\beta^2\left(B_r+G_r-2\frac{\partial p}{\partial x}\right)-\\&20Dah^4\beta^4N_b(1+DaM^2)+24h^2Da^2\beta^4(B_rN_t+B_rN_b+G_rN_b)+Da^2\beta^2N_bG_r(N_t+N_b)(8h^4\beta^4+3)\Big]-\frac{h^2N_bz^6}{15}\{Da\beta^4G_r[4Da\beta^2(N_t+N_b)-\\&(1+\lambda_1)(1+DaM^2)]-Da\beta^2B_r(1+\lambda_1)(1+DaM^2)-(1+DaM^2)[(1+\lambda_1)(1+DaM^2)(y^2-1)-2Da\beta^2]\}+\\&Dah\beta^4N_bz^3\left(\frac{z^2}{10}-\frac{1}{3}\right)[4Da\beta^2G_r(N_t+N_b)-(1+\lambda_1)(1+DaM^2)(B_r+G_r)]-\\&\frac{z^2}{4}\Big\{Da^2\beta^2N_b[G_rN_b+4h^2\beta^2B_r(1+2N_t)]+(1+\lambda_1)(1+DaM^2)\Big[DaN_b\beta^2(2h^2B_r+G_r)(2h^2\beta^2-1)+4h^4(1+DaM^2)(y^2-1)+\\&4h^2Da\beta^2\frac{\partial p}{\partial x}\Big]-2h^4Da^2(1+DaM^2)\Big\}\end{aligned}\quad \dots (26)$$

$$\begin{aligned}&\theta=\beta^2(z^2-h^2)+\frac{h-z}{2h}+\frac{1}{24}[24h^2\beta^2+(8h^4\beta^4+3)(N_t+N_b)]-\frac{1}{24}h\beta^2(N_t+N_b)z+\frac{z^2}{8h^2}(8h^2\beta^2+N_t+N_b)+\frac{(N_t+N_b)\beta^2}{3h}(z^3-h\beta^2z^4)-\\&\frac{h^4\beta^4}{45}\left[15(3N_t+2N_b)+4h^2\beta^2\left(N_b^2+2N_t^2+3N_tN_b\right)\right]+\frac{z}{720h}\left[120h^2\beta^2(3N_t+2N_b)+(16h^4\beta^4+15)\left(N_b^2+2N_t^2+3N_tN_b\right)\right]-\\&\frac{z^3}{6}\left[24h^2\beta^2(3N_t+2N_b)+(3-16h^4\beta^4)\left(N_b^2+2N_t^2+3N_tN_b\right)\right]+2h\beta^2z^4\left[4h^2\beta^2(3N_t+2N_b)+\left(N_b^2+2N_t^2+3N_tN_b\right)\right]-\frac{\beta^2}{60h}\left(N_b^2+2N_t^2+\right.\\&\left.3N_tN_b\right)\left(5hz^2+8\beta^2z^5-\frac{16}{3}h\beta^4z^6\right)\end{aligned}\quad \dots (27)$$

$$\Omega = \beta^2(z^2-h^2) + \frac{h-z}{2h} - \frac{\beta^2(N_t+N_b)}{N_b}(z^2-h^2) - \frac{N_t}{768h^4\beta^4 N_b}[768h^6\beta^6 + (1+96h^4\beta^4 + 256h^8\beta^8)(N_t+N_b)] + \frac{N_t(1+16h^4\beta^4)(N_t+N_b)z}{48h^3\beta^2 N_b} + \frac{N_t}{48h^3\beta^2 N_b}\left[48h^3\beta^4 z^2 + \frac{(N_t+N_b)}{16h\beta^2}(4h\beta^2 z-1)^4\right] \quad \ldots (28)$$

The volumetric flow rate q is

$$q = \int_0^{h(x)}\int_0^1 u(x,y,z)\,dydz \quad \ldots (29)$$

The average volume flow rate over one period $\left(T=\frac{\lambda}{c}\right)$ of the peristaltic wave is

$$Q = \int_0^{h(x)}\int_0^1 (u(x,y,z)+1)\,dydz = q + h(x) \quad \ldots (30)$$

From solving equation (30) after compensating the equation (29), the pressure gradient is obtained;

$$\frac{dp}{dx} = \frac{15Da}{h^3[2h^2(1+\lambda_1)^2(1+DaM^2)-5Da(1+\lambda_1)]}\left\{Q + \frac{h^3}{9\beta^2} - \frac{8h^5(1+\lambda_1)(1+DaM^2)}{45Da\beta^2} + \frac{68h^7(1+\lambda_1)(1+DaM^2)}{945Da\beta^2}(3\beta^2+2M^2) + + \frac{68h^7}{945Da^2\beta^2}[1 + 2\lambda_1 + \lambda_1^2(1+DaM^2)^2] - \frac{h^3 B_r(1+\lambda_1)}{10080Da}[1470Da + h^2(1+\lambda_1)(1+DaM^2)(1088h^2\beta^2-651)] - \frac{1}{10080Dah^3(1+\lambda_1)[1470Da+33DaN_t+DaN_t h^2\beta^2(102h^2\beta^2-84)+h^2(1+\lambda_1)(1+DaM^2)(1088h^2\beta^2-65)]}\right\} \quad \ldots (31)$$

Numerical integration of the pressure gradient along one wave, gives us a pressure rise Δp formula, i.e.

$$\Delta p = \int_0^1 \left(\frac{dp}{dx}\right) dx \quad \ldots (32)$$

The dimensionless friction force F at the wall per wavelength is given by:

$$F = \int_0^1 h\left(-\frac{dp}{dx}\right) dx \quad \ldots (33)$$

The corresponding stream function ψ can be obtained by integrating equation (26) with respect to z.

Results and Discussions:

Analytical solutions are acquired for momentum equation, energy equation and neutralizing the concentration of nano-particles with the help of homotopy perturbation technique up to the third order deformation. Discussed graphically all solutions obtained under variations of different parameters relevant in this section. The effects of side walls (aspect ratio β), amplitude ratio $\emptyset$, thermophoresis parameter N_t, average flow rate Q, Brownian movement parameter N_b, magnetic parameter M, local nanoparticle Grashof number B_r, Jeffrey fluid parameter λ_1, local temperature Grashof number G_r and Darcy number Da on the velocity u, temperature θ, nano-particles concentration ϑ, pressure rise Δp, pressure gradient $\frac{dp}{dx}$ and friction force F are presented by sketching graphs for three and two dimensions. The phenomenon of a trapped bolus is also incorporated by drawing streamlines for various physical parameters.

Based on equation (26), Figs. 2 - 6, illustrate the effect of the parameters $\emptyset, N_t, N_b, Q, M, B_r, \lambda_1, G_r, Da$ and β on the velocity. It is found that the velocity profile u, achieve its maximum height at z =0, the speed of the fluid begins to increase and tends to be fixed in the walls $\mp h(x)$ as particularly at the boundary conditions. Figure 2, illustrates the influence of the parameters $\emptyset$ and N_t on the velocity distribution function u vs. z. It is found that the velocity profile u rising up with the increasing $\emptyset$, when $|z| \le 1$, while u increases with increasing of N_t when z ∈ (-1,-0.4) ∪ (0.5,1), and u decreases with increasing N_t, when -0.4< z <0.5. Figure 3, shows the behavior of u under the variation of Q and N_b, one can depict here that u increases with the increasing of Q, while u increases with the increasing of N_b when -1< z <0.5, and u decreases with increasing N_b, when 0.5< z <1. Figure 4, contains the velocity profile behavior under the difference of M and B_r, it is aforesaid that the velocity profile rises with the increase of parameter M. The effect of the B_r parameter is similar to the parameter effect N_t on the velocity profile increases, where u increases with the increasing of B_r when z ∈ (-1,-0.5) ∪ (0.5,1), and u decreases with increasing B_r, when $|z| \le 0.5$. Figure 5, illustrates the effects of the parameters λ_1 and G_r on the velocity distribution function u vs. z. It is found that the velocity profile u rising up with the increasing of λ_1. Add to that, u goes down with the increasing G_r, when -0.35<z<0.55, and u increases with increasing B_r, when z ∈ (-1,-0.35) ∪ (0.55,1). Finally, Fig. 6 shows the velocity profile behavior under the variation of Q and Da. It is previously mentioned that the velocity profile goes down with the increasing effects of both the parameters. This appears to increase the extent of the side walls either by increasing the height of vertical or by reducing the horizontal distance of the walls, resulting in a decrease in fluid velocity.

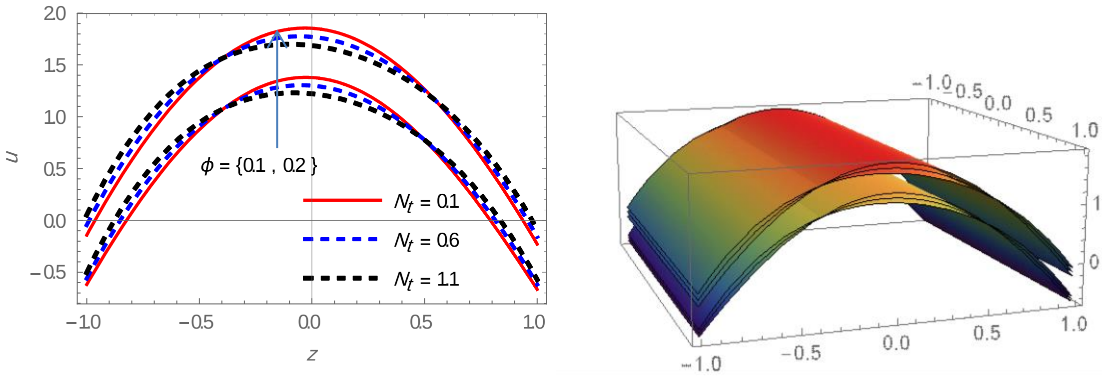

Figure 2. Velocity distribution for various values of $\emptyset$ and N_t with $x = 0, N_b = 0.5, Q = 1, B_r = 0.5, \lambda_1 = 0.6, G_r = 0.5, \beta = 1.5, Da = 0.9, M = 1.1$.

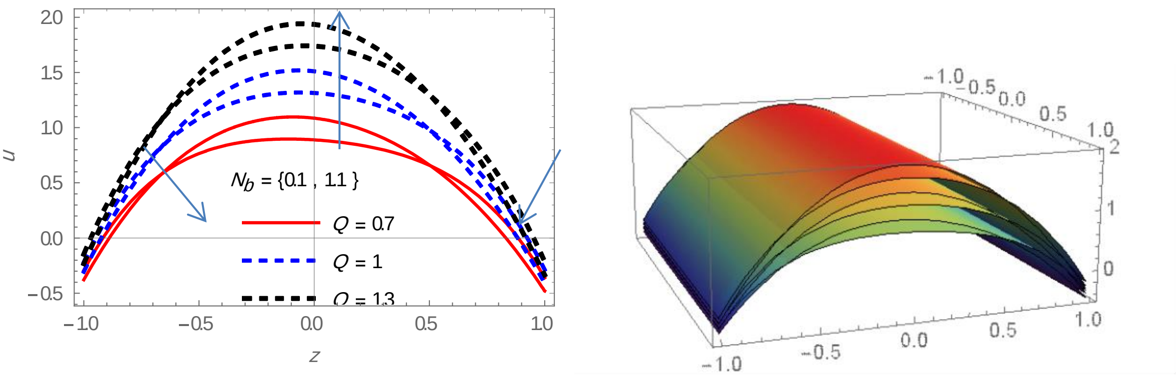

Figure 3. Velocity distribution for various values of Q and N_b with $x = 0, \emptyset = 0.15, N_t = 0.5, B_r = 0.5, \lambda_1 = 0.6, G_r = 0.5, \beta = 1.5, Da = 0.9, M = 1.1$.

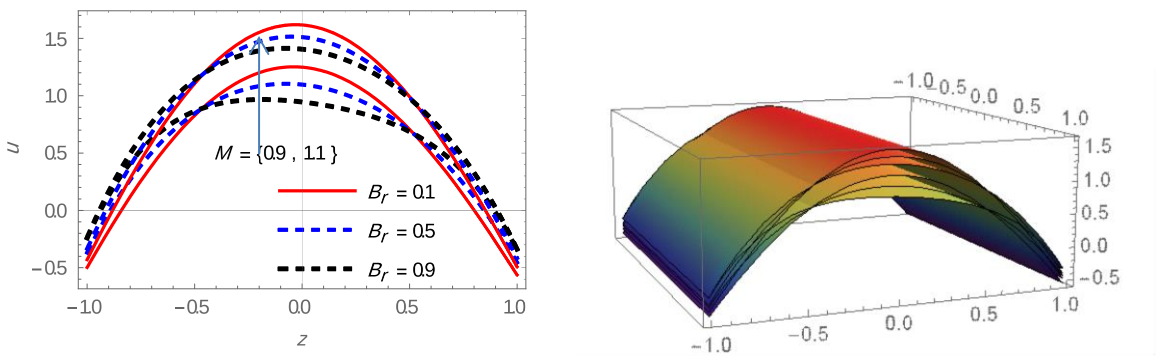

Figure 4. Velocity distribution for various values of M and B_r with $x = 0, \emptyset = 0.15, N_b = 0.5, N_t = 0.5, Q = 1, \lambda_1 = 0.6, G_r = 0.5, \beta = 1.5, Da = 0.9$.

Baghdad Science Journal

P-ISSN: 2078-8665
E-ISSN: 2411-7986

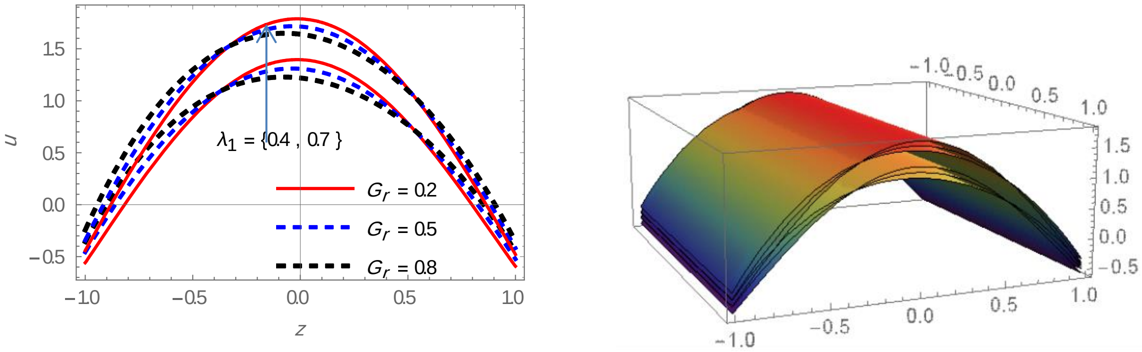

Figure 5. Velocity distribution for various values of λ_1 and G_r with $x = 0, \emptyset = 0.15, N_t = 0.5, N_b = 0.5, B_r = 0.5, Q = 1, \beta = 1.5, Da = 0.9, M = 1.1$.

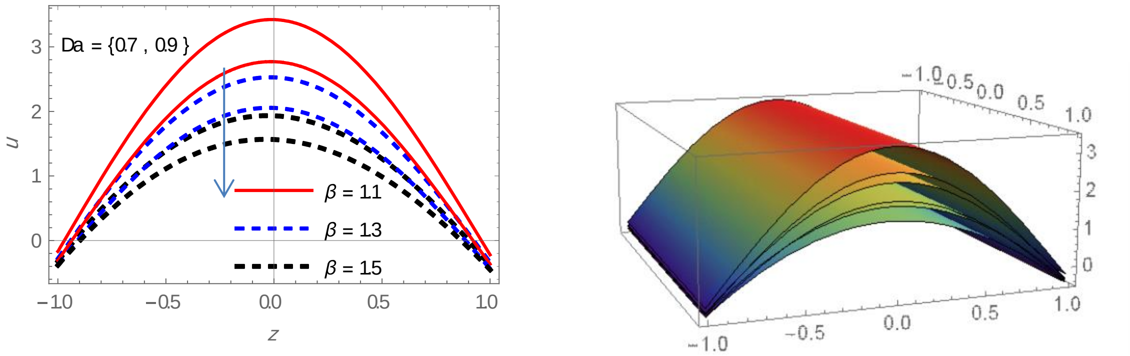

Figure 6. Velocity distribution for various values of Da and β with $x = 0, \emptyset = 0.15, N_t = 0.5, N_b = 0.5, B_r = 0.5, Q = 1, G_r = 0.5, \lambda_1 = 0.6, M = 1.1$.

Based on equation (27), Fig. 7, illustrates the effect of the parameters $\emptyset, \beta, N_b$ and N_t on the temperature distribution function θ. The graph for temperature curve along with the variations of the amplitude ratio $\emptyset$ and the lateral wall β with the other constant parameters are explained in (a). It is mentioned earlier that the velocity profile goes down with the increasing effects of both the parameters. Also, it is important to note that the temperature curve gives linear demeanor at $\beta = 0.3$ while for the large values of the side walls, the bending begins and gets its maximum curvature near *z* = -0.1 and disappears at *z* = *h(x)* to meet the physical quality at the walls. In (b), the temperature curve is a reduced function of N_b and N_t in the region -1.2< *z* <-0.3, while in -0.3< *z* <1.2, it shows opposite variation.

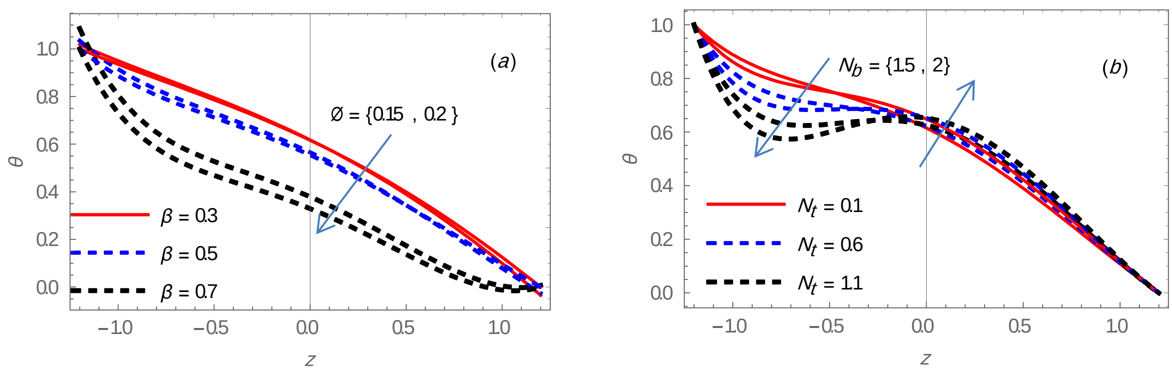

Figure 7. Temperature distribution θ vs. z with $x = 0, y = 1$, for (a) different values of $\emptyset$ and β at $N_t = 0.5, N_b = 0.5$, (b) different values of N_t and N_b at $\emptyset = 0.2, \beta = 0.5$.

Based on equation (28), Fig. 8 illustrate the effect of the parameters $\emptyset, \beta, N_b$ and N_t on the nanoparticles concentration Ω. The influence of the amplitude ratio $\emptyset$ and the lateral walls β on Ω can be measured from (a), the behavior of the concentration is almost similar to the behavior of temperature with variation $\emptyset$ and β. Whilst, it depicts that the concentration of nanoparticles is directly proportional to the difference of N_b but inversely related to N_t, view (b). From the figures below, observed the movement from - *h(x)* to 0, the curves are declined, but as proceed, those begin to rise and get stable in *h(x)*.

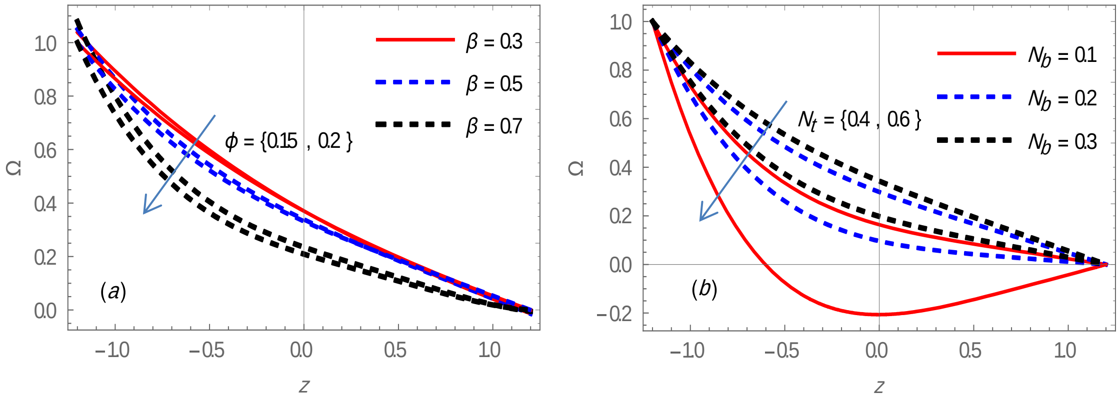

Figure 8. Temperature distribution Ω vs. z with $x = 0, y = 1, \emptyset = 0.2, \lambda_1 = 1$, for (a) different values of β at $N_t = 0.5, N_b = 0.5$, (b) different values of N_t and N_b at $\beta = 0.5$.

Based on equation (31), Fig. 9 illustrates the influence of the parameters $\emptyset, N_t, N_b, M, B_r, G_r, Da$ and β on the pressure gradient $\frac{dp}{dx}$ vs. x. The effects of the parameters M and N_b on the pressure gradient are explained in (a). It is found that $\frac{dp}{dx}$ rises with the increasing N_b, while $\frac{dp}{dx}$ goes down with the increasing M when 0.25<x<0.65 and $\frac{dp}{dx}$ rises with the increasing M, otherwise. Furthermore, if M = 1, $\frac{dp}{dx} \geq 0$ when 0.35<x<0.65 at N_b= 0.3, $\frac{dp}{dx} \geq 0$ when 0.32<x<0.68 at N_b= 0.4 and $\frac{dp}{dx} \geq 0$ when 0.3<x<0.7 at N_b= 0.5, otherwise $\frac{dp}{dx} \leq 0$. Also, observed that, if M= 1.2, $\frac{dp}{dx} \geq 0$ when 0.33<x<0.67 at N_b= 0.3, $\frac{dp}{dx} \geq 0$ when 0.31<x<0.69 at N_b= 0.4 and $\frac{dp}{dx} \geq 0$ when 0.3<x<0.7 at N_b= 0.5, otherwise $\frac{dp}{dx} \leq 0$. The influence of β and N_t on the pressure gradient can be noted from (b), it is mentioned here that $\frac{dp}{dx}$ goes down with the increasing effects of both the parameters β and N_t. Noted that, at β =1.3, $\frac{dp}{dx} \geq 0$, while if β =1.5, $\frac{dp}{dx} \geq 0$ when 0.23<x<0.77 at N_t= 0.4, $\frac{dp}{dx} \geq 0$ when 0.26<x<0.74 at N_t= 0.5, $\frac{dp}{dx} \geq 0$ when 0.28<x<0.72 at N_t= 0.6 and $\frac{dp}{dx} \leq 0$ otherwise. The influence of the parameters $\emptyset$ and Da on the pressure gradient is explained in (b). The pressure gradient is divided into two zones, positive and negative, under the variation of $\emptyset$ and Da. In the positive area, when 0.28<x<0.72, the effect of $\emptyset$ and Da on the pressure is direct, while in the negative region the effect is reversed. Finally (d), contains the behavior pattern of pressure gradient under the change of B_r and G_r. It is found that the pressure gradient goes down with the increasing effects of both parameters. Furthermore, if B_r=0.3, $\frac{dp}{dx} \geq 0$ when 0.1<x<0.9 at G_r=0.4 and $\frac{dp}{dx} \geq 0$ when 0.2<x<0.8 at G_r=0.5, otherwise $\frac{dp}{dx} \leq 0$, while if B_r= 0.5, $\frac{dp}{dx} \geq 0$ when 0.32<x<0.68 at G_r= 0.3, $\frac{dp}{dx} \geq 0$ when 0.28<x<0.72 at G_r= 0.4 and $\frac{dp}{dx} \geq 0$ when 0.2<x<0.8 at G_r= 0.5, otherwise $\frac{dp}{dx} \leq 0$.

Baghdad Science Journal

P-ISSN: 2078-8665
E-ISSN: 2411-7986

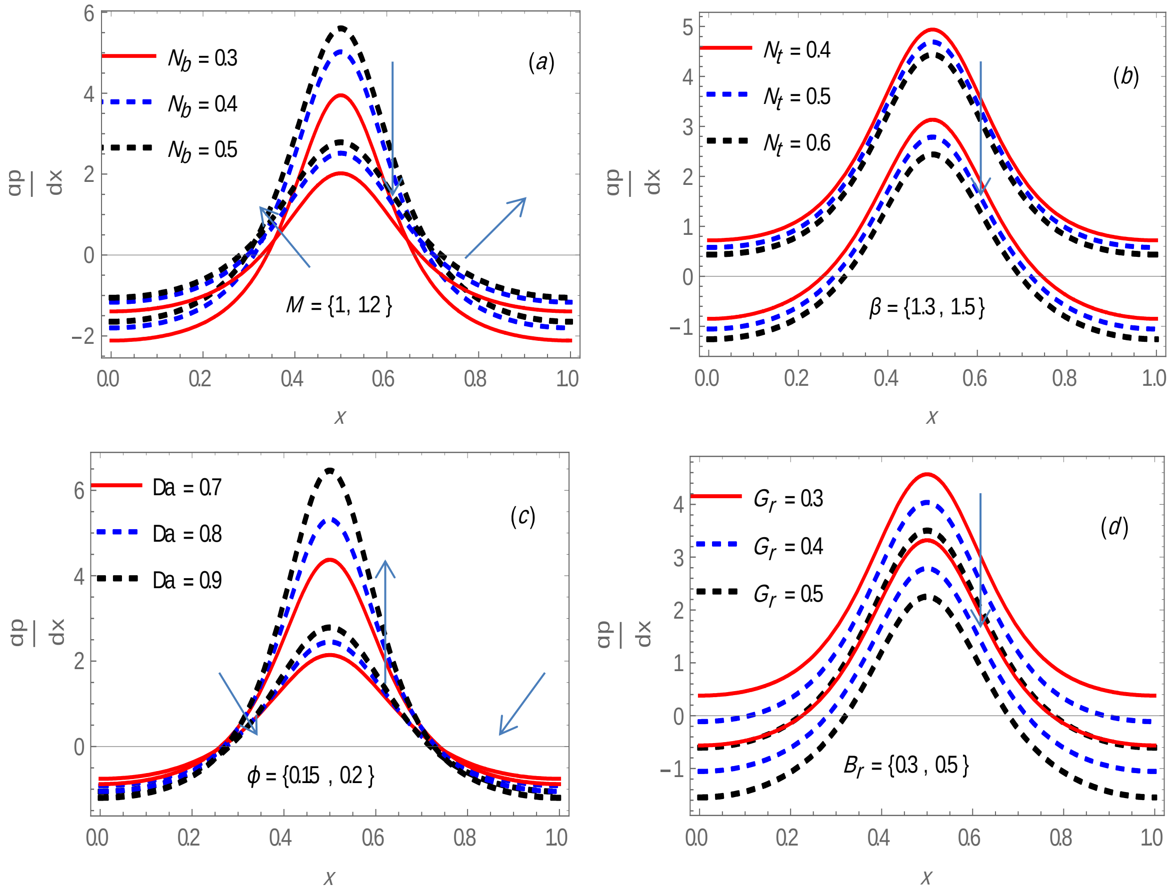

Figure 9. pressure gradient vs. z with $Q = 1, \lambda_1 = 1$, for (a) different values of $N_b$and M at $\emptyset = 0.15, N_t = 0.5, B_r = 0.5, Gr = 0.4, \beta = 1.5, Da = 0.9$, (b) different values of β and N_t at $\emptyset = 0.15,\ N_b = 0.5, N_b = 0.5, B_r = 0.5, Da = 0.9, M = 1.1$, (c) different values of $\emptyset$ and Da at $N_t = 0.5, N_b = 0.5, B_r = 0.5, Gr = 0.4, \beta = 1.5, M = 1.2$, (d) different values of B_r and Gr at $\emptyset = 0.15,\ N_t = 0.5, N_b = 0.5, \beta = 1.5, Da = 0.9, M = 1.2$.

Based on equation (32), Figs. 10 and 11, illustrates the effect of the parameters $B_r, \lambda_1, G_r, M, N_b, Da, N_t$ and β on the pressure rise Δp vs. $\emptyset$ and Q, respectively. Figure 10, illustrate the effect of the parameters $B_r, \lambda_1, G_r, M, N_b, Da, N_t$ and β on the pressure rise vs. $\emptyset$. The behavior of Δp vs. $\emptyset$, under the variation of B_r and λ_1 are explained in (a). One can depict here that Δp rises with the increasing λ_1, while Δp rises with the increasing B_r when 0<∅<0.4 and Δp goes down with the increasing B_r when 0.5<∅<1. Observed in (b), the influence of the parameters G_r and M on the pressure rise Δp vs. $\emptyset$. One can depict here that Δp goes down with the increasing M, while if M=1.2, Δp increases with the increasing of G_r, and if M=1, Δp decreases with increasing of G_r when 0<∅<0.4, and Δp increases with the increasing B_r when 0.4<∅<1. Observed in (c), that Δp rises with the increasing of both parameters N_b and Da. The behavior of Δp vs. $\emptyset$, under the variation of N_t and β are explained in (d). One can depict here that Δp goes down with the increasing N_t, while Δp rises with the increasing β. Furthermore, observed that the pressure rise function is generally increasing in (d), notice that at β=1.3 the function is increasing at the beginning and when it reaches the almost middle of the distance (∅=0.45) it begins to decrease.

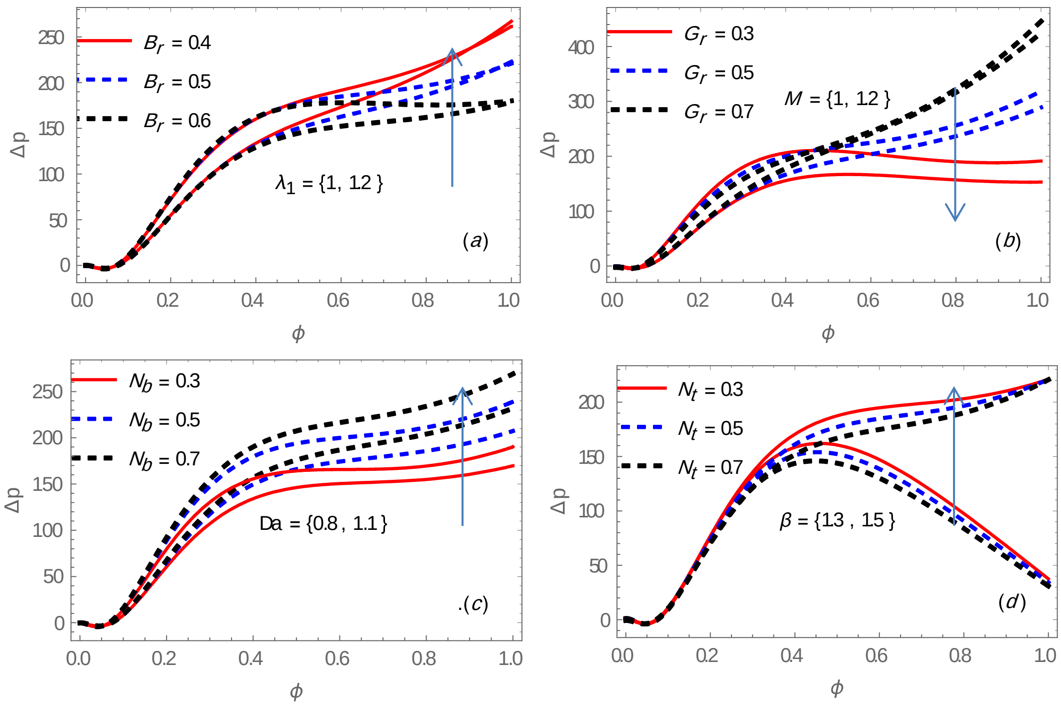

Figure 10. pressure rise Δp vs. $\emptyset$, at Q =1 for (*a*) different values of B_r and $\lambda_1$at $G_r = 0.4, M = 1.2, N_b = 0.5, N_t = 0.5,\ Da = 0.9, \beta = 1.5$, (*b*) different values of G_r and M at $B_r = 0.5, \lambda_1 = 1, N_b = 0.5, N_t = 0.5, Da = 0.9, \beta = 1.5$, (*c*) different values of N_b and Da at $B_r = 0.5, \lambda_1 = 1, G_r = 0.4, M = 1.2, N_t = 0.5, \beta = 1.5$, (*d*) different values of N_t and β at $B_r = 0.5, \lambda_1 = 1,\ N_b = 0.5, G_r = 0.4, M = 1.2, Da = 0.9$.

Figure 11 illustrates the effect of the parameters $B_r, \lambda_1, G_r, M, N_b, Da, N_t$ and β on the pressure rise Δp vs. Q. In (*a*) observed the influence of B_r and λ_1 on the pressure rise Δp vs. Q. One can depict here that Δp goes down with the increasing B_r, while if B_r=0.4, Δp increases with increasing of λ_1 when 0<Q<0.1, and Δp decreases with the increasing λ_1 when 0.1<Q<1, if B_r=0.5, Δp increases with increasing of λ_1 when 0<Q<0.15, and Δp decreases with the increasing λ_1 when 0.15<Q<1, and if B_r=0.6, Δp increases with increasing of λ_1 when 0<Q<0.2, and Δp decreases with the increasing λ_1 when 0.2<Q<1. Furthermore, if B_r= 0.4 obtaining Δp < 0 when Q < 0.1, if B_r= 0.5 obtaining Δp < 0 when Q < 0.15, and if B_r= 0.6 obtaining Δp < 0 when Q < 0.2, otherwise Δp > 0. Observed in (*b*), the behavior of Δp vs. Q, under the variation of G_r and M. Observed here that Δp goes down with the increasing G_r, while if G_r=0.3, Δp increases with increasing of M when 0<Q<0.3, and Δp decreases with the increasing M when 0.3<Q<1, if G_r=0.5, Δp increases with increasing of M when 0<Q<0.5, and Δp decreases with the increasing M when 0.5<Q<1, and if G_r=0.7, Δp increases with increasing of M when 0<Q<0.6, and Δp decreases with the increasing M when 0.6<$\emptyset$<1. Furthermore, at M=1.1, if G_r= 0.3 obtain the Δp < 0 when Q < 0.15, if G_r= 0.5 obtain the Δp < 0 when Q < 0.25, and if G_r= 0.7 obtain the Δp < 0 when Q < 0.3, otherwise Δp > 0. While at M=1.2, if G_r= 0.3 then Δp < 0 when Q < 0.1, if G_r= 0.5 then Δp < 0 when Q < 0.175, and if G_r= 0.7 then Δp < 0 when Q < 0.25, otherwise Δp > 0. In (*c*), observed that Δp rising up with the increasing of N_b, while if N_b=0.3, Δp decreases with increasing of Da when 0<Q<0.4, and Δp increases with the increasing Da when 0.4<Q<1, if N_b=0.5, Δp decreases with increasing of Da when 0<Q<0.25, and Δp increases with the increasing Da when 0.25<Q<1, if N_b=0.7, Δp decreases with increasing of Da when 0<Q<0.2, and Δp increases with the increasing Da when 0.2<Q<1. Furthermore, at Da=0.8, if N_b= 0.3 obtain Δp < 0 when Q < 0.2, if N_b= 0.5 obtain Δp < 0 when Q < 0.1, and if N_b= 0.7 obtain Δp < 0 when Q < 0.1, otherwise Δp > 0. While at Da=1.1, if N_b= 0.3 then Δp < 0 when Q < 0.275, if N_b= 0.5 then Δp < 0 when Q < 0.2, and if N_b= 0.7 obtain Δp < 0 when Q < 0.15, otherwise Δp > 0. Observed in (*d*), that Δp goes down with the increasing of both parameters N_t and β. Furthermore, at β=1.3, if N_t= 0.3 have Δp > 0, if N_t= 0.5 then Δp < 0 when Q < 0.05, and if N_t= 0.7 then Δp < 0 when Q < 0.1, otherwise Δp > 0. While at β=1.5, if N_t= 0.3 obtain Δp < 0 when Q < 0.1, if N_t= 0.5 have Δp < 0 when Q < 0.15, and if N_t= 0.7 then Δp < 0 when Q < 0.2, otherwise Δp > 0.

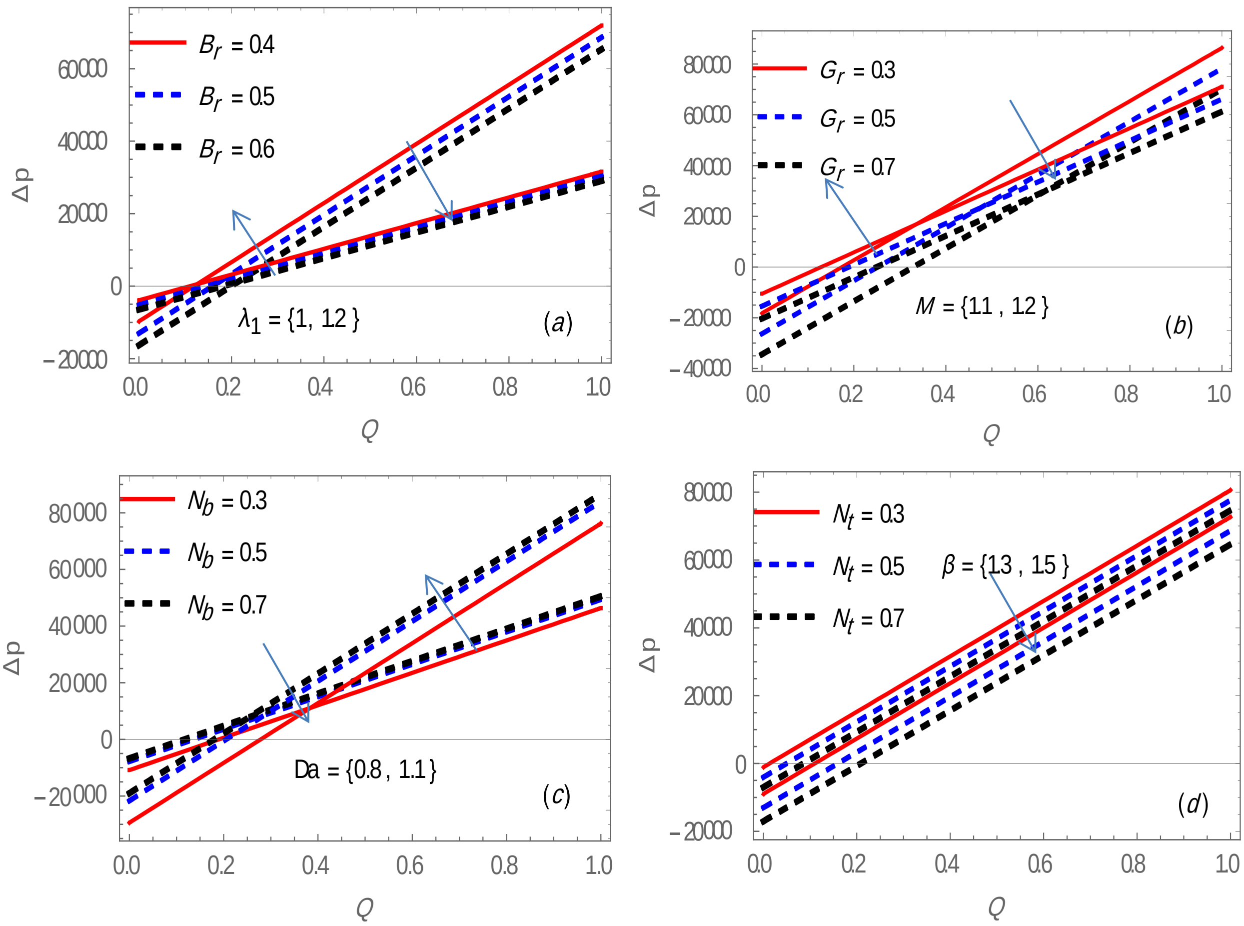

Figure 11. pressure rise Δp vs. Q, at $\emptyset$ =0.15 for (a) different values of B_r and $\lambda_1$at $G_r = 0.4, M = 1.2, N_b = 0.5, N_t = 0.5,\ Da = 0.9, \beta = 1.5$, (b) different values of G_r and M at $B_r = 0.5, \lambda_1 = 1, N_b = 0.5, N_t = 0.5, Da = 0.9, \beta = 1.5$, (c) different values of N_b and Da at $B_r = 0.5, \lambda_1 = 1, G_r = 0.4, M = 1.2, N_t = 0.5, \beta = 1.5$, (d) different values of N_t and β at $B_r = 0.5, \lambda_1 = 1,\ N_b = 0.5, G_r = 0.4, M = 1.2, Da = 0.9$.

Based on equation (33), Figs. 12 and 13 illustrate the effect of the parameters $B_r, \lambda_1, G_r, M, N_b, Da, N_t$ and β on the friction force F vs. $\emptyset$ and Q, respectively. Figure 12 illustrates the effect of the parameters $B_r, \lambda_1, G_r, M, N_b, Da, N_t$ and β on the friction force F vs. $\emptyset$. Observed that the distribution of friction force gives an inverse behavior compared to the distribution of pressure rise versus the amplitude ratio factor. Also, observed that the distribution of friction force gives an inverse behavior compared to the distribution of pressure rise versus the average flow rate Q in Fig. 13.

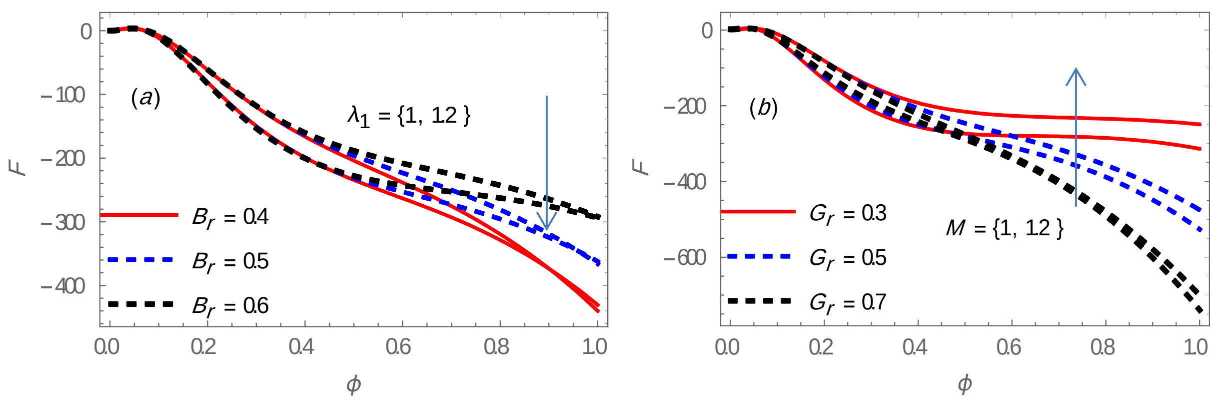

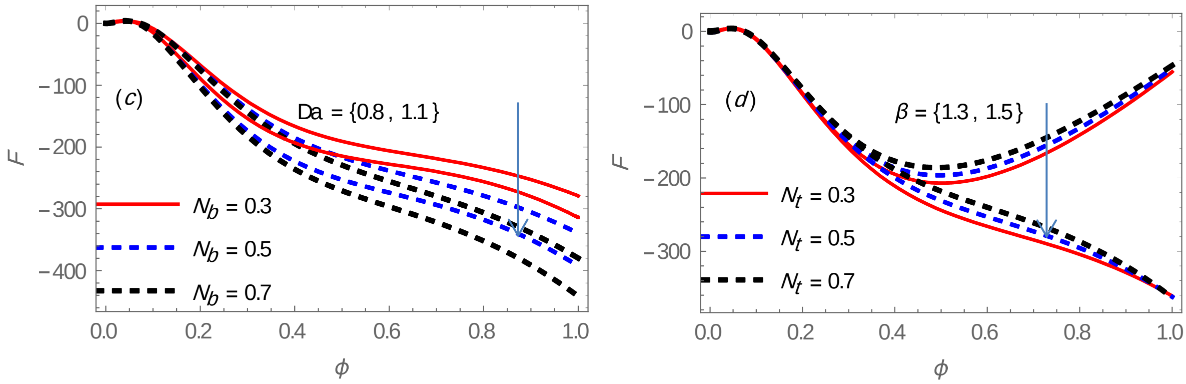

Figure 12. Friction force F vs. $\emptyset$, at Q =1 for (*a*) different values of B_r and $\lambda_1$at $G_r = 0.4, M = 1.2, N_b = 0.5, N_t = 0.5,\ Da = 0.9, \beta = 1.5$, (*b*) different values of G_r and M at $B_r = 0.5, \lambda_1 = 1, N_b = 0.5, N_t = 0.5, Da = 0.9, \beta = 1.5$, (*c*) different values of N_b and Da at $B_r = 0.5, \lambda_1 = 1, G_r = 0.4, M = 1.2, N_t = 0.5, \beta = 1.5$, (*d*) different values of N_t and β at $B_r = 0.5, \lambda_1 = 1,\ N_b = 0.5, G_r = 0.4, M = 1.2, Da = 0.9$.

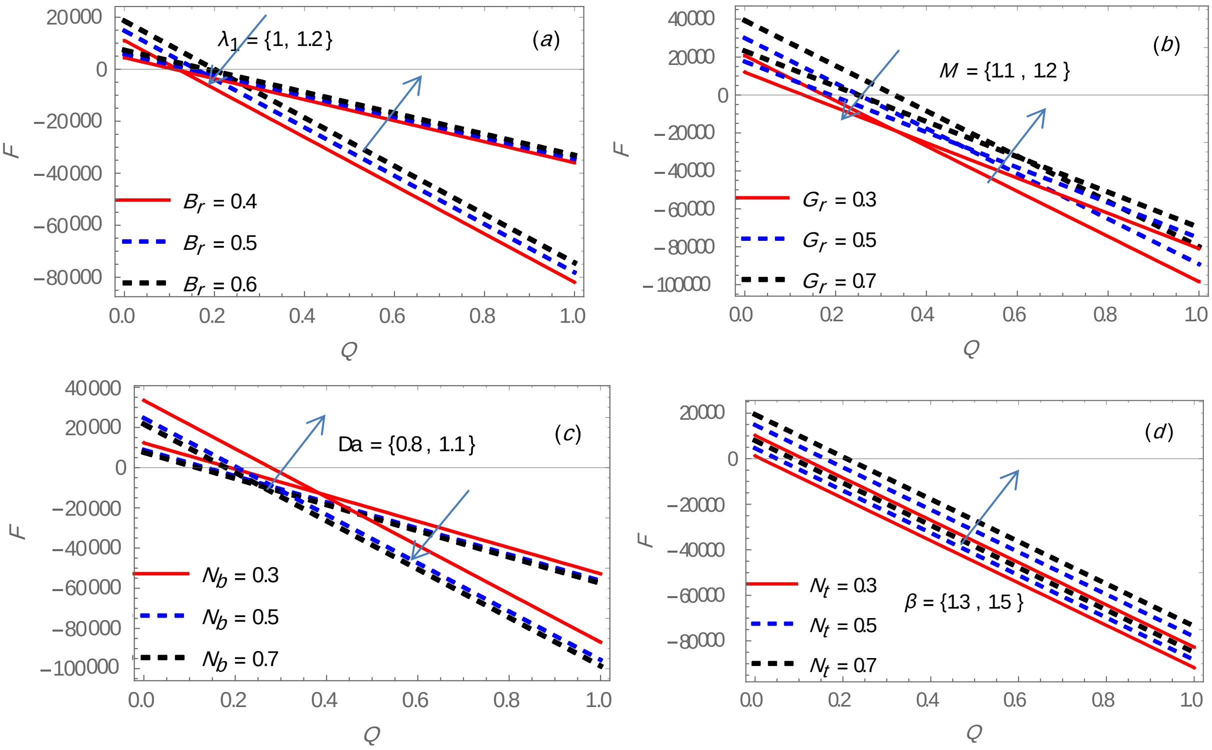

Figure 13. Friction force F vs. Q, at $\emptyset$ =0.15 for (*a*) different values of B_r and $\lambda_1$at $G_r = 0.4, M = 1.2, N_b = 0.5, N_t = 0.5,\ Da = 0.9, \beta = 1.5$, (*b*) different values of G_r and M at $B_r = 0.5, \lambda_1 = 1, N_b = 0.5, N_t = 0.5, Da = 0.9, \beta = 1.5$, (*c*) different values of N_b and Da at $B_r = 0.5, \lambda_1 = 1, G_r = 0.4, M = 1.2, N_t = 0.5, \beta = 1.5$, (*d*) different values of N_t and β at $B_r = 0.5, \lambda_1 = 1,\ N_b = 0.5, G_r = 0.4, M = 1.2, Da = 0.9$.

Trapping phenomena:

The effects of $\emptyset, \lambda_1, \beta, B_r, G_r, N_t, N_b, Q, M$ and Da on trapping bolus can be seen through Figs. 14 – 23. Figure 14 shows that the size of the trapped bolus grows and increases with the increasing of $\emptyset$, the effect of λ_1 on trapping bolus is similar to the effect of $\emptyset$ on trapping bolus which can be seen in Fig. 15. The effect of lateral walls on trapping bolus is analyzed in Fig. 16. It can be deduced that the size of the trapped bolus in the channel is contracted and decreases when β increases, also at β= 1.535 the upper bolus disappears while at β=1.5545 the lower bolus is disappeared. Figures 17 and 18 show that the size of the trapped bolus shrinks and decreases with the increases of B_r and G_r, respectively. The effect of thermophoresis parameter N_t on trapping bolus is analyzed in Fig. 19. It can be deduced that the size of the trapped bolus in the channel shrinks and decreases when N_t increases. While in Fig. 20 one can notice that the effect of the Brownian motion parameter N_b on trapping is inversion of effect of N_t on the trapped bolus. The effect of Q on the trapping is analyzed in Fig. 21, note that the dose size increases and expands with an increased Q. The effect of M on trapping analogous to effect Q on trapping, Observe that in Fig. 22. And the effect of Da on trapping bolus is analyzed in Fig. 23. It can be deduced that the size of the trapped bolus in the channel is contracted and decreases when Da increases, also at Da= 1.191 the upper bolus disappears while at Da= 1.241 the lower bolus disappears.

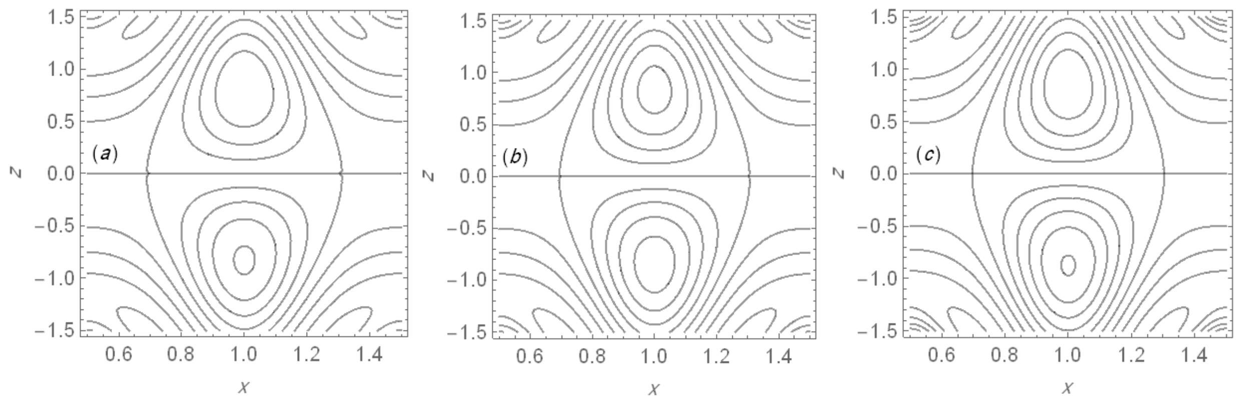

Figure 14. Streamlines for different values of ∅ at $y = 1, Q = 0.1, G_r = 0.3, M = 1.2, N_b = 0.5, N_t = 0.9, Da = 0.9,\ B_r = 0.3, \lambda_1 = 0.6, \beta = 1.2$ for: (*a*) ∅=0.15, (*b*) ∅=0.16 and (*c*) ∅=0.17.

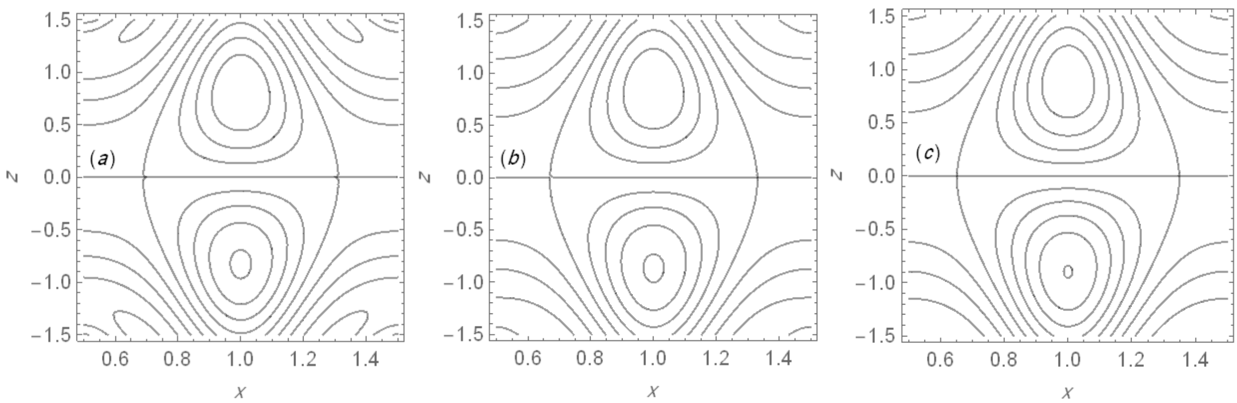

Figure 15. Streamlines for different values of λ_1 at $y = 1, Q = 0.1, G_r = 0.3, M = 1.2, N_b = 0.5, N_t = 0.9, Da = 0.9, B_r = 0.3, \emptyset = 0.15, \beta = 1.2$ for: (*a*) λ_1=0.6, (*b*) λ_1=0.7 and (*c*) λ_1=0.8.

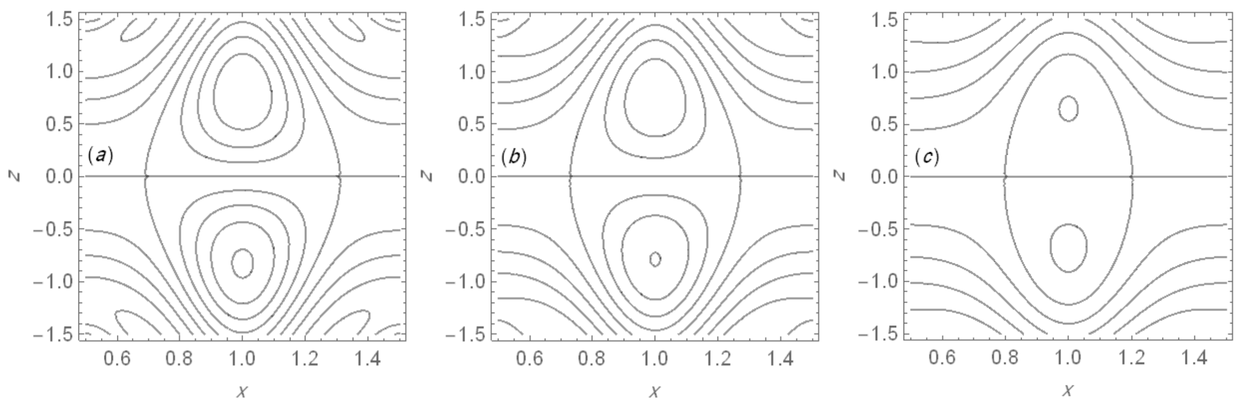

Figure 16. Streamlines for different values of β at $y = 1, Q = 0.1, G_r = 0.3, M = 1.2, N_b = 0.5, N_t = 0.9, Da = 0.9,\ B_r = 0.3, \emptyset = 0.15, \lambda_1 = 0.6$ for: (*a*) β=1.2, (*b*) β=1.3 and (*c*) β=1.53.

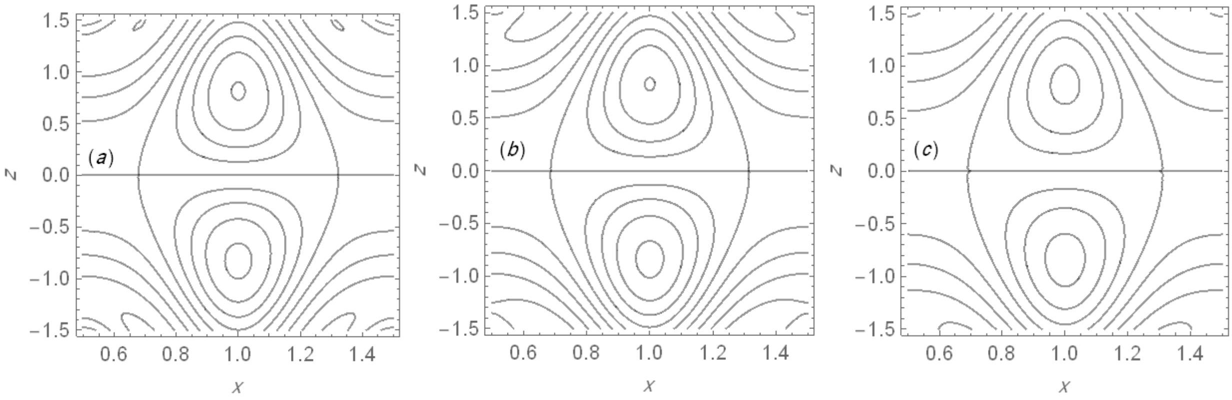

Figure 17. Streamlines for different values of B_r at $y = 1, Q = 0.1, G_r = 0.3, M = 1.2, N_b = 0.5, N_t = 0.9, Da = 0.9, \emptyset = 0.15, \lambda_1 = 0.6, \beta = 1.2$ for: (*a*) B_r=0.2, (*b*) B_r=0.3 and (*c*) B_r=0.5.

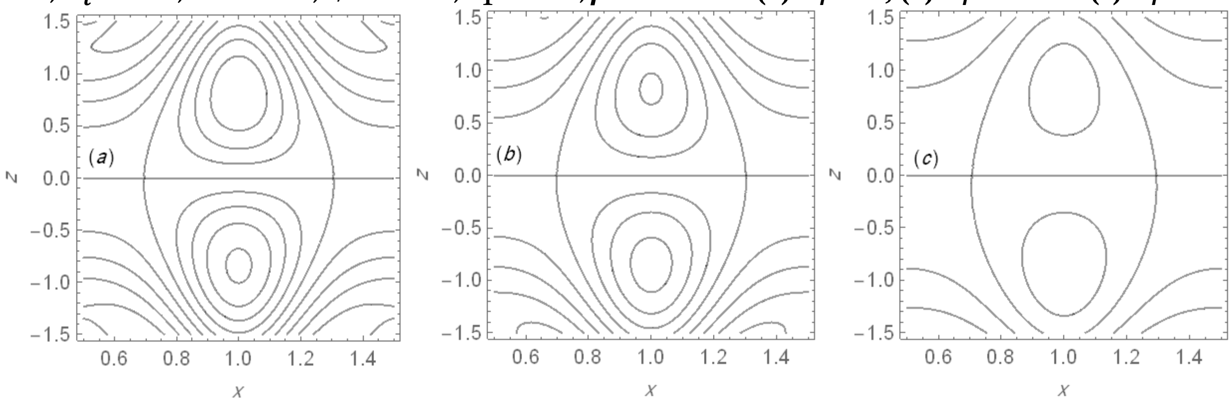

Figure 18. Streamlines for different values of G_r at $y = 1, Q = 0.1, B_r = 0.2, M = 1.2, N_b = 0.5, N_t = 0.9, Da = 0.9, \emptyset = 0.15, \lambda_1 = 0.6, \beta = 1.2$ for: (*a*) G_r=0.6, (*b*) G_r=0.7 and (*c*) G_r=1.

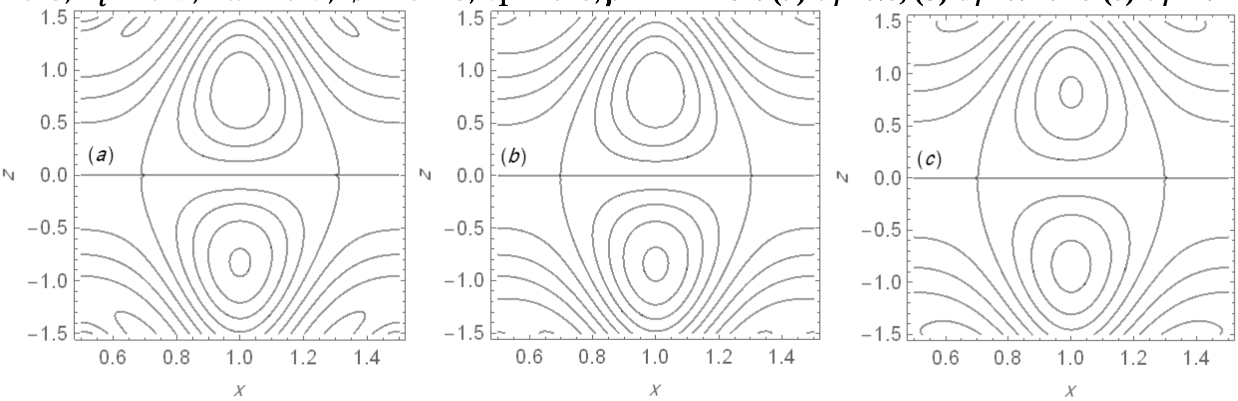

Figure 19. Streamlines for different values of N_t at $y = 1, Q = 0.1, B_r = 0.2, M = 1.2, N_b = 0.5, G_r = 0.3, Da = 0.9, \emptyset = 0.15, \lambda_1 = 0.6, \beta = 1.2$ for: (*a*) N_t=1, (*b*) N_t=1.5 and (*c*) N_t=2.

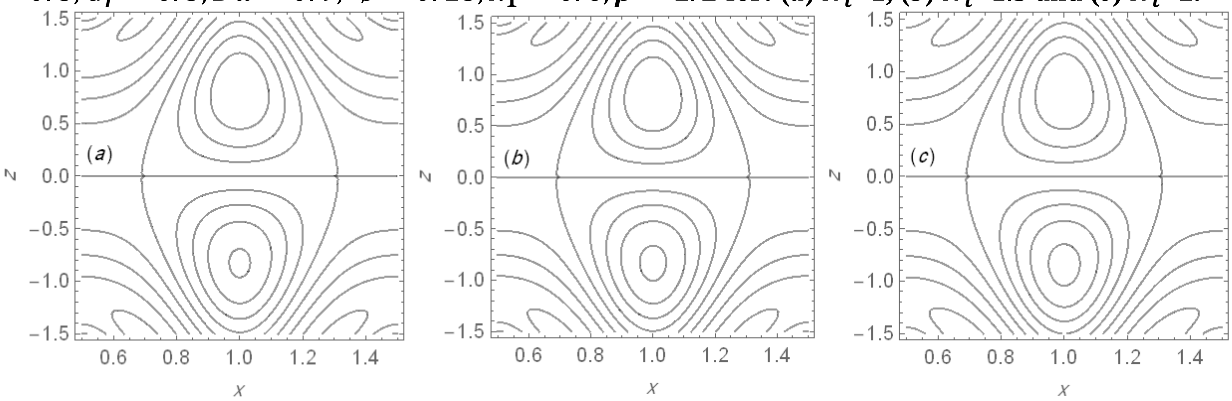

Figure 20. Streamlines for different values of N_b at $y = 1, Q = 0.1, B_r = 0.2, M = 1.2, N_t = 0.5, G_r = 0.3, Da = 0.9, \emptyset = 0.15, \lambda_1 = 0.6, \beta = 1.2$ for: (*a*) N_b=1, (*b*) N_b=1.5 and (*c*) N_b=2.

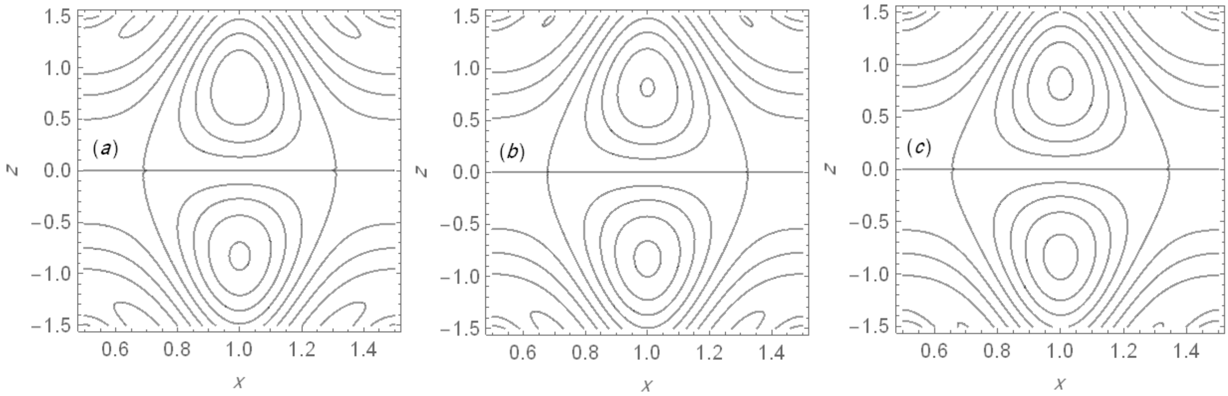

Figure 21. Streamlines for different values of Q at $y = 1, B_r = 0.2, M = 1.2, N_b = 0.5,, N_t = 0.5, G_r = 0.3, Da = 0.9,\ \emptyset = 0.15, \lambda_1 = 0.6, \beta = 1.2$ for: (*a*) Q=0.1, (*b*) Q=0.125 and (*c*) Q=0.15.

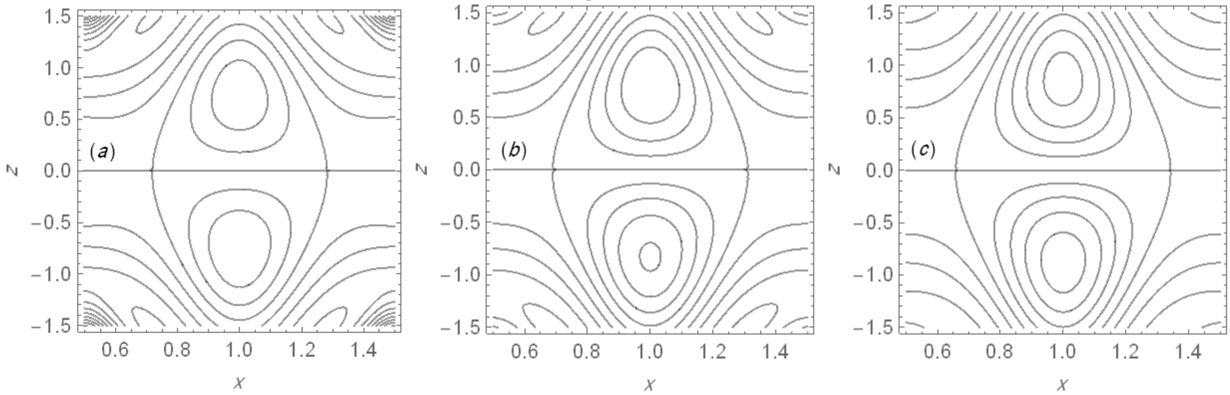

Figure 22. Streamlines for different values of M at $y = 1, Q = 0.1, B_r = 0.2, N_b = 0.5,, N_t = 0.5, G_r = 0.3, Da = 0.9,\ \emptyset = 0.15, \lambda_1 = 0.6, \beta = 1.2$ for: (*a*) M=1.2, (*b*) M=1.3 and (*c*) M=1.4.

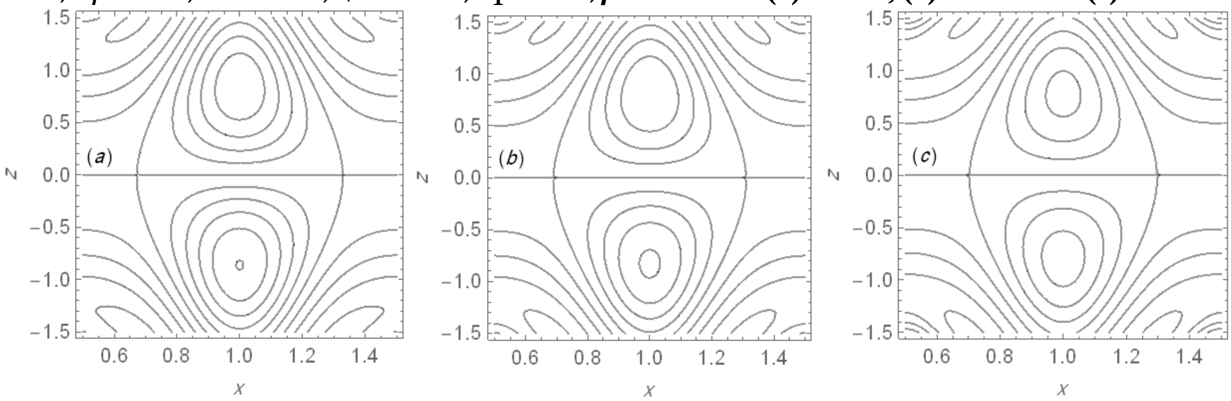

Figure 23. Streamlines for different values of Da at $y = 1, Q = 0.1, B_r = 0.2, N_b = 0.5,, N_t = 0.5, G_r = 0.3, M = 1.2,\ \emptyset = 0.15, \lambda_1 = 0.6, \beta = 1.2$ for: (*a*) Da=0.8, (*b*) Da=0.9 and (*c*) Da=1.19.

Concluding remarks:

The peristaltic flow of a nanofluid for Jeffrey fluid is deemed in a cross-section of rectangular porous medium duct to portray the mathematical results under convection is the phenomenon of heat transfer and the concentration of nanoparticles with the magnetic field. Current analysis can serve as a model that may help to understand the mechanism of physiological flows in a loop for fluids acting like nanofluids. From the mechanic's point of view, it is interesting to note how the peristaltic movement of the applied pressure gradient is affected. The exact expressions for axial velocity of the fluid, axial pressure gradient, pressure rise and stream function are obtained analytically. All governing equations are designed under the long wavelength approximation and the number of Reynolds negligible. The flow is measured in a reference frame moving at constant speed c along the axial direction of the canal. Analytical results were obtained using the HPM and all physical parameters affecting the phenomenon were discussed. The main findings can be summarized as follows:

1- The velocity is an increasing function vs. $\emptyset, Q, \lambda_1$ and M, respectively, but decreasing function vs. Da and β both for two and three dimensional analysis.

2- The velocity is a decreasing function vs. N_t, G_r and B_r, respectively, when -0.5 < z < 0.5, while the function is an increasing function when $z \in$ (-1,-0.5) ∪ (0.5,1).

3- The velocity is an increasing function vs. N_b when -0.5 < z < 0.5, while the function is a decreasing when z ∈ (-1,-0.5) ∪ (0.5,1).

4- The temperature distribution is changing inversely vs. $\emptyset$ and β, respectively. And the discussion previously mentioned that temperature curves decrease with increases in N_b and N_t when -1 < z < 0 while increases when 0 < z < 1, respectively.

5- The nanoparticles concentration rising up with the increase of N_b, while it reveals opposite relation with $\emptyset, N_t$ and β.

6- The pressure gradient profile displays direct relation with Q and N_b, while reverses variation with $\lambda_1, N_t, B_r, \beta$ and G_r. Also, the pressure gradient profile directs with Da and reverses with M in middle part of the canal, whilst in the both sides the fact is reversed. Furthermore the pressure gradient is positive in middle part of the canal, whilst negative on both sides of the canal.

7- The peristaltic pumping rate increases vs. $\emptyset$ with the increase in N_b, λ_1, G_r, Da and β, while decreases with the increase in B_r, N_t and M, respectively. Moreover, observed that the relationship between the pressure rise function and the amplitude ratio parameter is a parabola.

8- The peristaltic pumping rate decreases vs. the flux Q, with the increase in N_t, B_r, G_r and β, respectively, while increases with the increases of in N_b. Moreover, observed that the relationship between the pressure rise function and the flux is a linear. Also, it is concluded that peristaltic retrograde pumping (Δp<0) occurs when 0<Q<0.2, free pumping (Δp=0) occurs near Q=0.2 and peristaltic pumping region (Δp>0) occurs when Q>0.2.

9- The size of the trapped bolus is growing and increasing with the increasing of $\emptyset, N_b, \lambda_1, Q$ and M, respectively, while the trapped bolus is contracting and decreasing with increasing in β, N_t, B_r, G_r and Da. In general, the size of trapped bolus in upper half is greater than of lower half.

Author's declaration:

- Conflicts of Interest: None.
- I hereby confirm that all the Figures and Tables in the manuscript are mine. Besides, the Figures and images, which are not mine, have been given the permission for re-publication attached with the manuscript.
- Ethical Clearance: The project was approved by the local ethical committee in University of Al-Qadisiyah.

References:

1. Mishra M. Peristaltic Flows with Some Applications. PhD Thesis, Indian Institute of Science, Bangalore, 2004; pp9.
2. Kothandapani M, Srinivas S. Peristaltic transport of a Jeffrey fluid under the effect of magnetic field in an asymmetric channel. Int J Non Linear Mech. 2008;43(9):915–924.
3. Al-Khafajy DGS, Abdulhadi AM. Effects of wall properties and heat transfer on the peristaltic transport of a Jeffrey fluid through porous medium channel. Math. Theory Model., 2014;4(9):86–99.
4. Reddy M, Mishra M, Sreenadh S, Rao A. Influence of lateral walls on peristaltic flow in a rectangular duct. J. of F. Eng. 2005;127(4):824–827.
5. Nadeem S, Riaz A, Ellahi R, Akbar N. Mathematical model for the peristaltic flow of Jeffrey fluid with nanoparticles phenomenon through a rectangular duct. Appl Nanosci. 2014;4(5):613–624.
6. Nadeem S, Maraj EN. The mathematical analysis for peristaltic flow of nano fluid in a curved channel with compliant walls. Appl Nanosci, 2014;4(1):85–92.
7. Hayat T, Saleem A, Tanveer A, Alsaadi F. Numerical analysis for peristalsis of Williamson nanofluid in presence of an endoscope. Int. J. Heat Mass Transf. 2017;114:395–401.
8. Zin NA, Khan I, Shafie S, Alshomrani AS. Analysis of heat transfer for unsteady MHD free convection flow of rotating Jeffrey nanofluid saturated in a porous medium. Results Phys . 2017 Jan 1;7:288-309.
9. Latha R, Kumar BR. Effects of Thermal Radiation on Peristaltic Flow of Nanofluid in a Channel with Joule Heating and Hall Current. In Applied Mathematics and Scientific Computing. 2019 (pp. 301-311). Birkhäuser, Cham.
10. Hayat T, Farhat B, Farooq S, Khan A. Nonlinear radiative peristaltic flow of Jeffrey nanofluid with activation energy and modified Darcy's law. J BRAZ SOC MECH SCI. 2019 Jul 1;41(7):296.
11. Ansari Md, Motsa S, Trivedi M. Time Dependent Boundary Layer Flow and Heat Transfer of Jeffrey Nanofluid with Viscous Dissipation Effect. J. of Nanofluids, ASP. 2019;8(7):1458-1467.
12. Mehmood R, Nadeem S, Saleem S, Noreen SA. Flow and heat transfer analysis of Jeffery nano fluid impinging obliquely over a stretched plate. J Taiwan Inst Chem Eng. 2017;74: 49–58.

تأثير تباين درجة الحرارة والتركيز على الانتقال التمعجي للهيدروديناميكا الممغنطة لمائع جيفري مع ظاهرة الجسيمات النانوية خلال قناة مسامية مستطيلة

ضياء غازي صالح الخفاجي

قسم الرياضيات، كلية العلوم، جامعة القادسية، الديوانية، العراق.

الخلاصة:

تم إنشاء نموذج رياضي لدراسة الآثار المشتركة للتركيز والانتشار الحراري على الجسيمات النانوية لمائع جيفري مع تأثير المجال المغنطيسي على عملية احتواء الأمواج في قناة متوسطة مسامية مستطيلة ثلاثية الأبعاد. استخدمنا تقنية الاضطراب الهوموتوبي لحل المعادلات التفاضلية الجزئية اللاخطية. تم الحصول على نتائج عددية لتوزيع درجة الحرارة، تركيز الجسيمات النانوية، السرعة، ارتفاع الضغط، تدرج الضغط، قوة الاحتكاك ودالة التدفق. من خلال الرسوم البيانية، وجدت أن سرعة المائع مباشرة مع معدل متوسط لتدفق الحجم والمعلمة المغناطيسية بينما تكون عكسية مع عدد دارسي والجدران الجانبية. أيضا، تتصرف السرعة بشكل غريب تحت تأثير معلمة الحركة البراونية وتأثير عدد كراشوف النانوي المحلي.

الكلمات المفتاحية: طريقة الاضطراب الهوموتوبي (HPM)، مائع جيفري، مجال مغناطيسي هيدروديناميكي، جسيمات نانوية، تدفق تمعجي.